



UNIVERSITÉ LIBRE DE BRUXELLES

SUMMARY

**Aerodynamics
MECA-Y402**

Author:
Enes ULUSOY

Professor:
Herman DECONINCK

Year 2016 - 2017

Appel à contribution

Synthèse Open Source



Ce document est grandement inspiré de l'excellent cours donné par Herman DECONINCK à l'EPB (École Polytechnique de Bruxelles), faculté de l'ULB (Université Libre de Bruxelles). Il est écrit par les auteurs susnommés avec l'aide de tous les autres étudiants et votre aide est la bienvenue ! En effet, il y a toujours moyen de l'améliorer surtout que si le cours change, la synthèse doit être changée en conséquence. On peut retrouver le code source à l'adresse suivante

<https://github.com/nenglebert/Syntheses>

Pour contribuer à cette synthèse, il vous suffira de créer un compte sur *Github.com*. De légères modifications (petites coquilles, orthographe, ...) peuvent directement être faites sur le site ! Vous avez vu une petite faute ? Si oui, la corriger de cette façon ne prendra que quelques secondes, une bonne raison de le faire !

Pour de plus longues modifications, il est intéressant de disposer des fichiers : il vous faudra pour cela installer L^AT_EX, mais aussi *git*. Si cela pose problème, nous sommes évidemment ouverts à des contributeurs envoyant leur changement par mail ou n'importe quel autre moyen.

Le lien donné ci-dessus contient aussi un README contenant de plus amples informations, vous êtes invités à le lire si vous voulez faire avancer ce projet !

Licence Creative Commons

Le contenu de ce document est sous la licence Creative Commons : *Attribution-NonCommercial-ShareAlike 4.0 International (CC BY-NC-SA 4.0)*. Celle-ci vous autorise à l'exploiter pleinement, compte-tenu de trois choses :



1. *Attribution* ; si vous utilisez/modifiez ce document vous devez signaler le(s) nom(s) de(s) auteur(s).
2. *Non Commercial* ; interdiction de tirer un profit commercial de l'œuvre sans autorisation de l'auteur
3. *Share alike* ; partage de l'œuvre, avec obligation de rediffuser selon la même licence ou une licence similaire

Si vous voulez en savoir plus sur cette licence :

<http://creativecommons.org/licenses/by-nc-sa/4.0/>

Merci !

Contents

1	2D wings in compressible flow	1
1.1	Subsonic flows	1
1.1.1	The Prandtl-Glauert relation	1
1.1.2	Improved corrections for compressibility	4
1.1.3	The critical Mach number	5
1.2	Transonic flows	6
1.2.1	Drag divergence Mach number	6
1.2.2	Supercritical wings	8
1.3	Supersonic flows	8
1.3.1	The drag coefficient in a linearized supersonic flow	8

Chapter 1

2D wings in compressible flow

1.1 Subsonic flows

1.1.1 The Prandtl-Glauert relation

Remind that we have defined a potential function to describe incompressible flows, conservation of mass giving:

$$\vec{v} = \nabla\phi \quad \frac{\partial u}{\partial x} + \frac{\partial v}{\partial y} = 0 = \frac{\partial^2\phi}{\partial x^2} + \frac{\partial^2\phi}{\partial y^2}. \quad (1.1)$$

This can also be used to describe compressible flows, conservation of mass is then:

$$\rho(\phi_{xx} + \phi_{yy}) + \rho_x\phi_x + \rho_y\phi_y = 0 \quad (1.2)$$

where we introduced the shorthand notation $\frac{\partial a}{\partial x} = a_x$. We assume that the flow is isentropic, this is satisfied by inviscid flows (no shock wave):

$$\frac{\rho}{T^{\frac{1}{\gamma-1}}} = cst \quad \Rightarrow \frac{d\rho}{\rho} = \frac{1}{\gamma-1} \frac{dT}{T} \quad (1.3)$$

if the flow does not work (turbine), the temperature is constant and the equation becomes:

$$d\rho = -\frac{\rho}{2a^2}d(u^2 + v^2). \quad (1.4)$$

If we replace the velocities we get:

$$\rho_x = -\frac{\rho}{a^2}(\phi_x\phi_{xx} + \phi_y\phi_{xy}) \quad \rho_y = -\frac{\rho}{a^2}(\phi_x\phi_{xy} + \phi_y\phi_{yy}). \quad (1.5)$$

That we can substitute in (1.2):

$$\left(1 - \frac{1}{a^2}\phi_x^2\right)\phi_{xx} + \left(1 - \frac{1}{a^2}\phi_y^2\right)\phi_{yy} - \frac{2}{a^2}\phi_x\phi_y\phi_{xy} = 0. \quad (1.6)$$

We can now apply this to an airfoil, if the far field velocity profile is $u = V_\infty$, we can note the velocity field by means of perturbations: $u = V_\infty + \hat{u}$, $v = \hat{v}$. A perturbation potential function can be defined:

$$\phi = V_\infty x + \hat{\phi} \quad \text{with} \quad \hat{\phi}_x = \hat{u}, \quad \hat{\phi}_y = \hat{v}. \quad (1.7)$$

By substitution of this in (1.6):

$$\left[a^2 - (V_\infty + \hat{\phi}_x)^2 \right] \hat{\phi}_{xx} + \left[a^2 - \hat{\phi}_y^2 \right] \hat{\phi}_{yy} - 2(V_\infty + \hat{\phi}_x) \hat{\phi}_y \hat{\phi}_{xy} = 0. \quad (1.8)$$

Since the total temperature is constant:

$$\frac{a_\infty^2}{\gamma - 1} + \frac{V_\infty^2}{2} = \frac{a^2}{\gamma - 1} + \frac{(V_\infty + \hat{u})^2}{2} = \hat{v}^2 \quad (1.9)$$

If we make the assumption of small perturbation, the quadratic terms cancel and (1.8) and (1.9) become:

$$\begin{aligned} \frac{a_\infty^2}{a^2} &= 1 - (\gamma - 1) \frac{\hat{u}}{V_\infty} M_\infty^2 \\ \left[a^2 - V_\infty^2 + 2V_\infty \hat{u} \right] \hat{\phi}_{xx} + a^2 \hat{\phi}_{yy} - 2V_\infty \hat{v} \hat{\phi}_{xy} &= 0 \\ \Rightarrow \left[1 - M_\infty^2 - (\gamma + 1) M_\infty \frac{\hat{u}}{V_\infty} \right] \hat{\phi}_{xx} + \left[1 - (\gamma - 1) M_\infty^2 \frac{\hat{u}}{V_\infty} \right] \hat{\phi}_{yy} - 2M_\infty^2 \frac{\hat{v}}{V_\infty} \hat{\phi}_{xy} &= 0 \end{aligned} \quad (1.10)$$

where the last expression is obtained by dividing by a_∞^2 and replacing. By considering again the small perturbation ($V_\infty \ll$) equation we get the:

Transonic small perturbation potential equation

$$\left[(1 - M_\infty^2) - (\gamma + 1) M_\infty^2 \frac{\hat{\phi}_x}{V_\infty} \right] \hat{\phi}_{xx} + \hat{\phi}_{yy} = 0. \quad (1.11)$$

We can see that the \hat{u} appears in $\hat{\phi}_{xx}$ term, this is no longer negligible for **sonic** velocities. For sub- and super-sonic flows however the equation simplifies in:

$$(1 - M_\infty^2) \hat{\phi}_{xx} + \hat{\phi}_{yy} = 0. \quad (1.12)$$

Note that we retrieve our incompressible equation for $M_\infty \rightarrow 0$. Be aware that this last relation is only valid for small perturbations (small bodies in practice) and sub- or super-sonic flows ($M_\infty > 1.2$, $M_\infty < 0.8$).

Let's now operate a change of coordinate $(x, y) \rightarrow (\xi, \eta)$, recalling $1 - M_\infty^2 \equiv \beta^2$:

$$\xi = x \quad \eta = \beta y \quad \bar{\phi}(\xi, \eta) = m \cdot \hat{\phi}(x, y) \quad (1.13)$$

where m is a constant. Let's find the expression of $\bar{\phi}(\xi, \eta)$. The chain rule gives:

$$\begin{aligned} \hat{\phi}_x &= \hat{\phi}_\xi = \frac{1}{m} \bar{\phi}_\xi & \hat{\phi}_y &= \frac{\beta}{m} \bar{\phi}_\eta & \hat{\phi}_{xx} &= \frac{1}{m} \bar{\phi}_{\xi\xi} & \hat{\phi}_{yy} &= \frac{\beta^2}{m} \bar{\phi}_{\eta\eta} \\ \Rightarrow \bar{\phi}_{xx} + \bar{\phi}_{yy} &= 0 \end{aligned} \quad (1.14)$$

We can see that the compressible flow in (x, y) is reduced to an incompressible flow in the (ξ, η) plane. Pay attention that $\bar{\phi}$ describes the perturbation velocities \bar{u}, \bar{v} in the (ξ, η) plane.

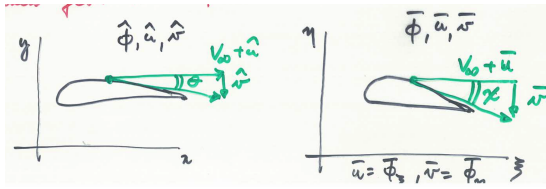


Figure 1.1

We can now focus on the shape of the profile in the new axis. Let's analyze the tangent to the profile by defining the angle θ for the profile in (x, y) . Under the assumption of small perturbation (thin airfoil), we can see that:

$$\tan \theta \approx \theta = \frac{\hat{v}}{V_\infty + \hat{u}} \approx \frac{\hat{v}}{V_\infty} = \frac{1}{V_\infty} \hat{\phi}_y \quad \Rightarrow \chi \approx \frac{1}{V_\infty} \bar{\phi}_\eta \quad (1.15)$$

where the analogy for the new plane is done. Using (1.14), we get:

$$\theta = \frac{\beta}{m} \chi. \quad (1.16)$$

Let's investigate two cases:

- If we choose $m = \beta$, $\theta = \chi$, the two profiles are identical. We have for the velocity:

$$\hat{u} = \hat{\phi}_x = \frac{\bar{\phi}_\xi}{\beta} = \frac{\bar{u}}{\beta} \quad (1.17)$$

and since the pressure coefficient is given by $C_p = -\frac{2\hat{u}}{V_\infty}$:

Prandtl-Glauert rule

$$C_p = \frac{C_{p,inc}}{\beta} = \frac{C_{p,inc}}{\sqrt{1 - M_\infty^2}}. \quad (1.18)$$

This equation allows us to compute the pressure distribution in compressible flow, beginning from the incompressible one.

Since the lift and moment coefficient are given by the integration of the pressure coefficient along the wing, we have the same result for them (so also the slope of lift curve m). Here is plotted the experimental data and the approximated m by means of the above relation for $\alpha = 0$ and for different airfoil thickness τ . We can see that for the thinner wings, we have a good agreement, until we reach the **critical Mach number** (Mach number at infinity for which Mach number 1 is reached on the profile). This value exceeded, we have shock waves (formula valid only for Mach until 0.8). For thicker wings, we see that the slope m is always underestimated. The critical Mach number is here much lower.

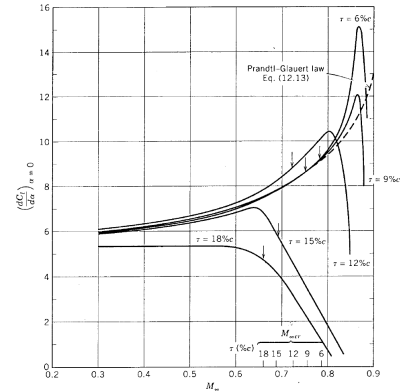


Figure 1.2

- If we choose $m = 1$, $\hat{u} = \bar{u}$ so that $C_p = C_{p,inc}$. We see that the pressure coefficient is now the same but the profiles are different following we are in the compressible or incompressible case $\theta = \beta\chi$.



The angle relation must be true along the entire profile, particularly at the maximum thickness:

$$\tau = \beta\tau_{inc}. \quad (1.19)$$

Figure 1.3

Remark 1 If we take into account the aspect ratio, we can rewrite the slope m as:

$$m = \frac{m_{inc}}{\beta} \frac{2\pi}{\beta \left(1 + \frac{2}{eAR}\right)} \quad (1.20)$$

where we used the theoretical 2D slope 2π . Another possibility is to write the lift as:

$$c_l = \frac{2\pi}{\beta} (\alpha - \alpha_{L_0} - \alpha_i) = \frac{2\pi}{\beta + \frac{2}{eAR}} (\alpha - \alpha_{L_0}) \quad (1.21)$$

We can last note the existence of the DATCOM formula that accounts for the effect of the aspect ratio, sweep angle Λ , Mach number and has also a correction factor for viscous effects $\kappa \approx 0.97$:

$$m = \frac{2\pi AR}{2 + \sqrt{\frac{AR^2 + beta^2}{\kappa^2} \left(1 + \frac{\tan^2 \Lambda}{\beta^2}\right) + 4}}. \quad (1.22)$$

Remark 2 We can also rearrange the expression of C_p with the approximation of small angles, we had:

$$C_p = \frac{p - p_\infty}{\frac{1}{2} \rho_\infty V_\infty^2} = \frac{\gamma 2 p_\infty}{\gamma \rho_\infty V_\infty^2} \left(\frac{p}{p_\infty} - 1\right) = \frac{2}{\gamma M_\infty^2} \left(\frac{p}{p_\infty} - 1\right) \quad \gamma \frac{p_\infty}{\rho_\infty} = \gamma r T = a^2 \quad (1.23)$$

The isentropic flow and the constant T_c give:

$$\begin{aligned} \frac{p}{p_\infty} &= \left(\frac{T}{T_\infty}\right)^{\frac{\gamma}{\gamma-1}} = \left(\frac{T_t - \frac{1}{2c_p} [(V_\infty + \hat{u})^2 + \hat{v}^2]}{T_\infty}\right)^{\frac{\gamma}{\gamma-1}} \quad T_t = T_\infty + \frac{V_\infty^2}{2c_p} \\ \Rightarrow \frac{p}{p_\infty} &= \left[1 - \frac{\gamma-1}{2} M_\infty^2 \left(\frac{2\hat{u}}{V_\infty} + \frac{\hat{u}^2 + \hat{v}^2}{V_\infty^2}\right)\right]^{\frac{\gamma}{\gamma-1}} = 1 - \frac{\gamma}{2} M_\infty^2 \left(\frac{2\hat{u}}{V_\infty} + \frac{\hat{u}^2 + \hat{v}^2}{V_\infty^2}\right) + \dots \end{aligned} \quad (1.24)$$

where the last expression comes from the fact that the second term is small so that we have the Taylor development of $1 + \epsilon$ (first order limited). We can neglect the second term in bracket since we have small perturbation square, and we get by (1.23):

$$\frac{p}{p_\infty} = -\frac{2\hat{u}}{V_\infty} \quad (1.25)$$

1.1.2 Improved corrections for compressibility

With the increasing cruise speed of WW2, we have 2 more precise relations:

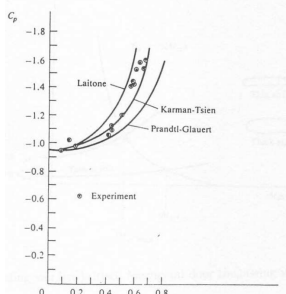
Karman-Tsien relation

$$C_p = \frac{C_{p,inc}}{\sqrt{1 - M_\infty^2} + \frac{M_\infty^2}{1 + \sqrt{1 - M_\infty^2}} \frac{C_{p,inc}}{2}} \quad (1.26)$$

or the more recent:

Laitone relation

$$C_p = \frac{C_{p,inc}}{\sqrt{1 - M_\infty^2} + \frac{M_\infty^2 (1 + \frac{\gamma-1}{2} M_\infty^2) C_{p,inc}}{2\sqrt{1 - M_\infty^2}}} \quad (1.27)$$



We can see experimental results here, using these coefficient we match better the lower values.

1.1.3 The critical Mach number

By definition, it is the M_∞ when $M = 1$ somewhere on the airfoil. Consider a point A, the drag is given by Figure 1.4

$$C_{p,A} = \frac{2}{\gamma M_\infty^2} \left(\frac{p_A}{p_\infty} - 1 \right) \quad (1.28)$$

If we combine the fact that the flow is isentropic:

$$\frac{p_A}{p_\infty} = \left(\frac{T_A}{T_\infty} \right)^{\frac{\gamma-1}{2}} = \left(\frac{1 + \frac{\gamma-1}{2} M_\infty^2}{1 + \frac{\gamma-1}{2} M_A^2} \right)^{\frac{\gamma}{\gamma-1}} \Rightarrow C_{p,A} = \frac{2}{\gamma M_\infty^2} \left[\left(\frac{1 + \frac{\gamma-1}{2} M_\infty^2}{1 + \frac{\gamma-1}{2} M_A^2} \right)^{\frac{\gamma}{\gamma-1}} - 1 \right] \quad (1.29)$$

If now we consider $M_\infty = M_{kr} \rightarrow M_A = 1$, so that the equation becomes:

$$C_{p,A} = \frac{2}{\gamma M_\infty^2} \left[\left(\frac{1 + \frac{\gamma-1}{2} M_\infty^2}{1 + \frac{\gamma-1}{2} M_A^2} \right)^{\frac{\gamma}{\gamma-1}} - 1 \right] \quad C_{p,A} = \frac{C_{p,A,inc}}{\sqrt{1 - M_{kr}^2}}, \quad (1.30)$$

where the second equation is the Prandtl-Glauert relation. We can plot the two equations on a graph. The intersection of the two graphs gives the critical Mach number. We can see that the minimum lift coefficient at low velocities is more negative than the thin case, characterized by a smaller M_{kr} . The perturbation of the flow is higher. Flying at high subsonic velocities is important \rightarrow thin airfoil. When the angle of attack increases, the lift increases but the higher velocity on the suction part makes the M_{kr} much lower. We want so the wing to be as thin as possible but we are limited by the structural strength and the fuel storage.

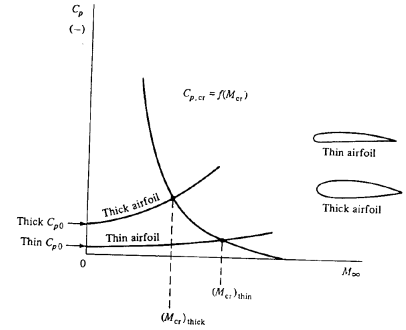


Figure 1.5

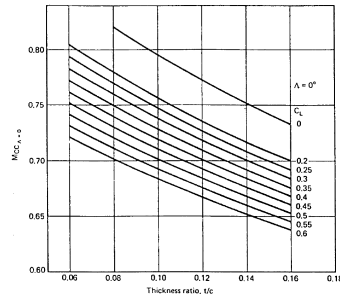


Figure 1.6

We avoid also large bending of the leading edge to avoid large accelerations. One solution to increase M_{kr} is to place the maximum camber downstream, about 50% of the chord because the velocities on the suction side will be lower. Placing it too downstream will create a too high opposite gradient and cause separation.

Symmetrical wings have a larger M_{kr} , however be careful with combination of sharp LE because of LE separation. In practice we have a quasi-symmetrical profile with camber near LE. **Swept** wings also increase the M_{kr} .

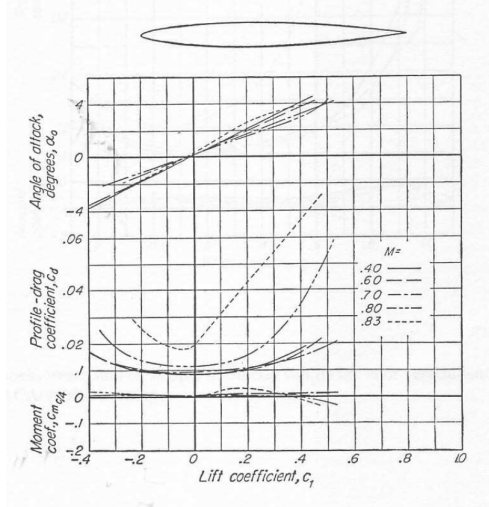


Figure 1.7

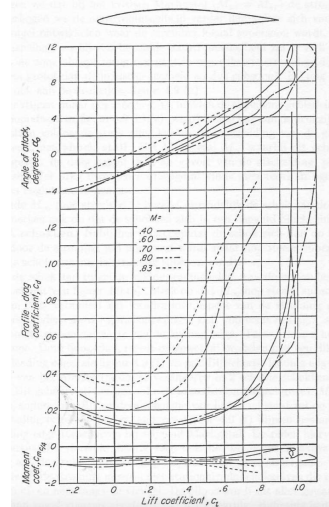


Figure 1.8

We can observe here above, the plot of α , C_L and C_D for a symmetrical and a non-symmetrical airfoil. We can observe on Figure 1.7 that the slope of the lift curve goes up to $M = 0.83$ (Prandtl-Glauert). Once above M_{kr} it starts to decrease and the drag suddenly increases.

On Figure 1.8 we can see similar effects at the difference that around M_{kr} we have a positive increase of the zero lift angle, having a negative effect on longitudinal stability. Note that the decrease of the lift curve starts earlier, M_{kr} is smaller.

1.2 Transonic flows

1.2.1 Drag divergence Mach number

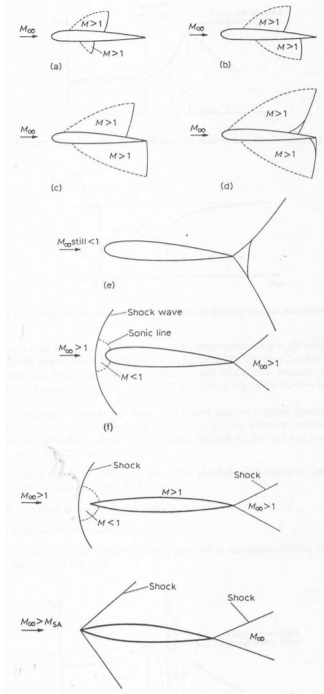


Figure 1.9

At the critical Mach number $M_\infty = M_{cr}$, the flow reaches $M = 1$ somewhere on the wing. If the velocity at ∞ is increased, M_∞ also (still <0), a small area where the flow becomes **supersonic** will develop on the **suction side**. For increasing M_∞ this area will grow and at a certain M_∞ a **shock wave** will develop, as a result of which the flow will become **subsonic** again (the supersonic area abruptly terminated). Such area also develops on the **pressure side** at high M_∞ (Figure 1.9 (a)).

If M_∞ increases further, the supersonic regions further extends and the shock waves move downstream, the one on the pressure side more rapidly (Figure 1.9 (b) (c)). As soon as the shock waves are strong enough, they can cause separation of the boundary layer, this separation is the **shock stall** and the M_∞ where this happens is called the **drag divergence Mach number**. Indeed, the drag suddenly increases as a result of the separation, this called **transonic drag rise**, shown on Figure 1.10.

For further increase of $M_\infty < 1$, the shock wave on the pressure side eventually reaches the trailing edge (Figure 1.9 (d)). In a certain Mach number range, the shock wave manifests the so-called

λ shocks. Near the profile the shock has two legs, a first oblique one through which the flow is slowed down but remains supersonic, and a second normal one through which the flow becomes subsonic.

Eventually the shock wave on the suction side can also reach the trailing edge and give birth to the **bifurcated trailing edge shock pattern** (Figure 1.9 (e)).

For further increase of M_∞ there is no change, till M_∞ exceeds 1. In this case, a so-called **detached bow shock** develops upstream of the leading edge. There is a small subsonic region between this shock and the leading edge. This manifests both for thick, bounded leading edge and thin one (Figure 1.9 (f) (g)). In the second case, the bow shock changes into 2 oblique shocks at the leading edge for increasing M_∞ (Figure 1.9 (h)). This happens at the **shock attachment Mach number, M_{SA}** . For further M_∞ , the flow becomes fully supersonic and the drag decreases. In the case of rounded leading edge, the bow shock continues to exist and comes closer to the leading edge.

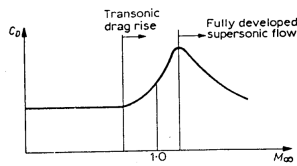


Figure 1.10

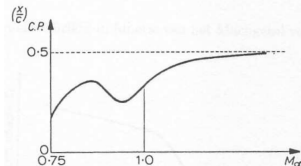


Figure 1.11

Under transonic conditions the flow is non-stationary, the shock waves moves up and down on the wing. The pilot senses this as **buffeting** (response of the structure to aerodynamic excitation) and vibrations. This can make the plane uncontrollable or cause serious damages. The cause of the excitation is the fluctuating pressure in non-stationary conditions. Normally one flies under the buffeting margin but one can exceed it in case of sudden maneuvers for fighters for example.

The center of pressure is also moving with M_∞ (Figure 1.11). First, it goes backward as the shock wave going backward on the suction side makes the underpressure greater. Then, it goes forward because the shock wave on the pressure side is moving faster. The latter reaches the trailing edge while the shock wave on the suction side still moves backward, making the center of pressure again move backward, tending to the 50% chord. This makes the control of the plane more difficult.

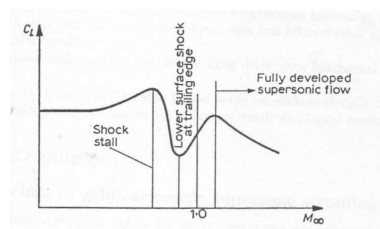


Figure 1.12

It is this buffeting effect that imposes an upper limit to the velocity of subsonic planes. With the increase of the drag due to separation when shock waves (shock-stall) is associated a decrease of the lift. We can see that the lift temporary increases after the lower shock reaches the trailing edge. This is explained by the smaller separation when in this location. The drag divergence Mach number is 5-10% larger than M_{cr} .

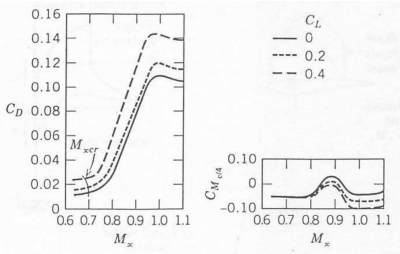


Figure 1.13

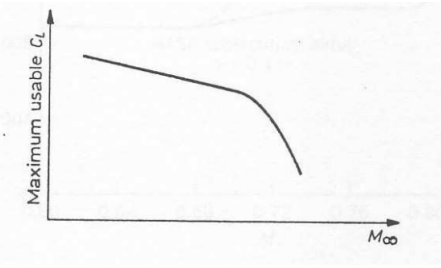


Figure 1.14

On Figure 1.13 we can see the influence of increasing lift (increasing α). We can notice that with increasing lift, the drag increases for all Mach numbers, the moment increases in the transonic region and M_{cr} decreases. On Figure 1.14, we notice that the lift coefficient strongly decreases in the transonic region due to buffering effects.

1.2.2 Supercritical wings

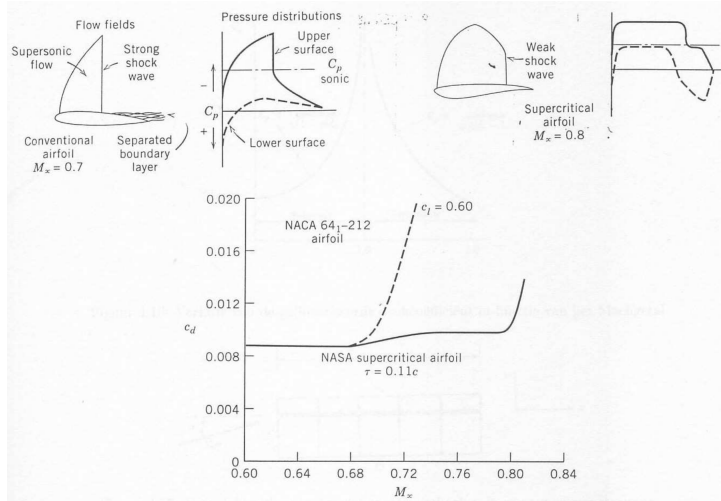


Figure 1.15

closer to the trailing edge.

For subsonic wings, it is thus desired to have the largest drag divergence Mach number possible. This can be achieved by using high critical Mach number wings, or increase the difference $M_{div} - M_{cr}$. The second solution led to the supercritical wings. These have a rather flat suction side to limit the acceleration of the flow, keeping the supersonic speeds lower than other profiles and limit the strength of the shock that creates less drag. The comparison between the two type of wings is done on Figure 1.15. We can see that the M_{cr} is higher and the weaker shock wave

The new shape of the suction side has a negative effect on the lift, this is compensated by an increased curvature on the pressure side near the trailing edge. On the figure we can see that the use of critical wings increases the drag divergence Mach number, that can go up to 0.99. These allows the use of thicker wings, allowing more fuel storage at lower speeds.

1.3 Supersonic flows

1.3.1 The drag coefficient in a linearized supersonic flow

The potential equation we used in the framework of potential equation can be rewritten in the case of supersonic flow as:

$$(1 - M_\infty^2) \hat{\phi}_{xx} + \hat{\phi}_{yy} = 0 \quad \Rightarrow \lambda^2 \hat{\phi}_{xx} - \hat{\phi}_{yy} = 0. \quad (1.31)$$

The linearized potential equation corresponds to the wave equation with $\lambda^2 = M_\infty^2 - 1 > 0$. We can show that the solution of this equation is

$$\hat{\phi}(x, y) = f(x\lambda y) = \hat{\phi}_1(x - \lambda y) + \hat{\phi}_2(x + \lambda y). \quad (1.32)$$

Let's define 2 families of characteristic curves:

$$\begin{cases} C^+ : x - \lambda y = cst & \Rightarrow y = \frac{1}{\lambda}x + cst = \frac{1}{\sqrt{M_\infty^2 - 1}}c + cst \\ C^- : x + \lambda y = cst & \Rightarrow y = -\frac{1}{\lambda}x + cst = -\frac{1}{\sqrt{M_\infty^2 - 1}}c + cst \end{cases} \quad (1.33)$$

In this way, $\hat{\phi}_1$ and $\hat{\phi}_2$ are respectively constant on C^+ and C^- .

The slope is denoted μ_∞^\pm for C^\pm such that:

$$\tan \mu_\infty^\pm = \pm \frac{1}{\sqrt{M_\infty^2 - 1}} \quad \sin \mu_\infty^\pm = \pm \frac{1}{M_\infty}. \quad (1.34)$$

To find the general solution in P, let's first consider the initial data given on the y-axis:

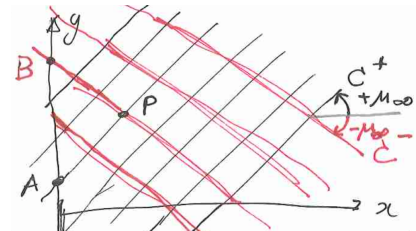


Figure 1.16

$$\hat{\phi}_1(y) = F(y) \quad \hat{\phi}_2(y) = G(y) \quad (1.35)$$

Now let's construct C^+ and C^- through P:

$$C^+ : x - \lambda y = x_A - \lambda y_A \quad C^- : x - \lambda y = x_B + \lambda y_B. \quad (1.36)$$

Finally, the solution in P is so given by:

$$\hat{\phi}(x_p, y_p) = \hat{\phi}(x_A - \lambda y_A) + \hat{\phi}_2(x_B + \lambda y_B) = F(x_A - \lambda y_A) + G(x_B + \lambda y_B) \quad (1.37)$$

Application to a flat plate